ROYAL SOCIETY OF CHEMISTRY

PAPER

Check for updates

DOTA complexes with divalent zinc, cadmium and mercury: X-ray and solid-state NMR studies and solution isomerism

Jakub Obuch, [ID] [a,b] Ivana Císařová,[a] Jiří Brus [ID] *[b] and Petr Hermann [ID] *[a]

DOTA is widely regarded as a "prototype chelator" in the coordination chemistry of macrocyclic ligands. Its macrocyclic cavity can adapt to the size and coordination requirements of various metal ions. However, its complexes with divalent metal ions have been less explored than those with trivalent ions. Here, we studied the complexes of d^{10} metal ions, Zn(II), Cd(II) and Hg(II), which are chemically similar but have different ionic radii and prefer different coordination numbers (CNs). Solid-state structures of the $[M(dota)]^{2-}$ anions show different coordination modes going from an octahedron and CN 6 for Zn(II) to a twisted-square antiprismatic (TSA) arrangement with CN (6 + 2) for Cd(II) and CN (6 + 1)/(6 + 2) for Hg(II). The coordination spheres are distorted from the ideal arrangements, and they consist of four amine groups (forming an N_4 plane) and 2–4 oxygen atoms of the carboxylate pendant arms. The oxygen atoms of the pendant arms are also bound to Ba(II) or Ca(II) counter-ions in various metal-ion bridging modes. The ^{13}C and ^{15}N solid-state NMR data correspond well to the structures determined by X-ray diffraction. The fluxionality of the coordination sphere was investigated by variable-temperature ^{13}C NMR spectroscopy in solution. The measurements pointed to a higher rigidity of the macrocycle chelate rings compared to those formed by the pendant arms. The pendants are highly fluxional due to the easy change of their coordination modes as was observed in the solid state. Overall, the results confirm the size-dependent coordination behaviour of the internal cavity of DOTA-like macrocycles, which differs significantly from those observed in complexes of trivalent metal ions, *e.g.* trivalent lanthanides.

Introduction

Macrocyclic ligands and their complexes are employed in various medicinal applications. Gadolinium(III) complexes are used as the most common MRI contrast agents.[1,2] If the co-ordinated metal ion is a suitable radioactive nuclide, the resulting complex can be used as a PET or SPECT tracer[3,4] or as a therapeutic radiopharmaceutical agent.[5] Fluorescent complexes have also been used as optical probes in molecular imaging.[6,7] Among the parent polyaza macrocycles, cyclen (1,4,7,10-tetraazadodecane) derivatives frequently modified on their four nitrogen atoms (*e.g.* the tetraacetate derivative DOTA and its analogues) are the most common chelators found in these applications. The applicability of these macrocyclic complexes in medicine can be illustrated using an MRI contrast agent Dotarem®,[8] a PET tracer for neuroendocrine tumours ^{68}Ga–DOTATOC[9] often paired with the ^{177}Lu-containing thera-peutic drug Lutathera®[10] or the prostate cancer therapeutic drug Pluvicto® containing ^{177}Lu.[11]

The macrocyclic cavities of DOTA derivatives are able to accommodate ions of almost all metal elements in the Periodic Table. The parent ligand, DOTA, is sometimes also referred to as a "prototype" macrocyclic chelator reflecting its general versatility and ability to form thermodynamically stable and kinetically inert complexes with such a diverse range of metal ions. The DOTA derivatives are octadentate ligands and, thus, their cavity is very suitable for lanthanide(III) ions or large metal ions, such as In(III), Pb(II) or Bi(III), able to coordinate all donor atoms of the ligands. In complexes of smaller ions of the first-row d-block elements, such as Cu(II) ions, or p-elements, *e.g.* Ga(III) ions, requiring octahedral coordination, the macrocycle amine groups and only two car-boxylate pendant arms are bound to the central metal ion. Complexes of DOTA derivatives with trivalent metal ions, mainly with Ln(III), have been thoroughly studied over more than 40 years.[12] Although the early DOTA studies dealt mostly with divalent metal ions, coordination chemistry of DOTA with divalent metal ions has been, surprisingly, much less investi-gated than that of trivalent metal ions over the years.

[a]Department of Inorganic Chemistry, Faculty of Science, Charles University, Hlavova 2030/8, 128 40 Prague 2, Czech Republic. E-mail: petrh@natur.cuni.cz
[b]Institute of Macromolecular Chemistry, Czech Academy of Science, Heyrovského náměstí 2, 162 00 Prague 6, Czech Republic. E-mail: brus@imc.cas.cz

Structures of complexes of pre-organized macrocyclic ligands with a "fixed" size of the ligand cavity depend significantly on the size and required/allowed coordination number of the metal ions. The influence of the size of the metal ions on complex properties is better investigated in a series of ions where no other parameters alter them. The divalent d^{10} metal ions of group-12 elements, Zn(II), Cd(II) and Hg(II), form such a series where the increase of the coordination number (CN) can be expected. Complexes of these metal ions with some cyclen derivatives with up to four coordinating pendant arms (accessible CN from six to eight) have been structurally investigated from this point of view.[12]

Structures of several Zn(II) complexes with cyclen derivatives have been determined by X-ray diffraction.[13–16] The Zn(II) ion is typically hexacoordinated in a distorted octahedral arrangement. Only a few structures exhibit higher coordination numbers (CNs). Thus, heptacoordinated complexes were observed for cyclen-tris(pyrazol) or cyclen-tris(acetamide) ligands,[17,18] and a square-antiprismatic arrangement with CN 8 was found only with a ligand having four weakly-bound tetrakis(methylphosphine-oxide) pendants and, thus, a large ligand cavity.[19] In the Zn(II) complex with DOTA itself, all cyclen amine groups and two acetate pendant arms are coordinated to the Zn(II) central metal ion (CN 6). Two protonated pendant arms remain uncoordinated and are engaged in hydrogen bonds with neighbouring complex units, thereby forming 1D chains.[20] Heavier Group 12 metal ions present more variable CNs in their complexes than the Zn(II) ion. Divalent cadmium has a small CN 5 in complexes of the cyclen derivative with no coordinating pendant arms, 1,4,7,10-tetrabenzyl-cyclen, complemented with a coordinated acetonitrile[21] or in a complex of the mono(methylene-*o*-phenol) cyclen derivative due to the steric hindrances induced by the ligand.[22] However, the Cd(II) ion generally prefers more donor atoms. The seven-coordinated Cd(II) is present in a complex with a cyclen-monoacetamide where the ligand donor atoms and two acetonitrile molecules are bound.[23] The binding mode of octadentate ligands is mostly derived from a twisted square antiprismatic (TSA) arrangement. A 6 + 2 coordination is more common than others and it has been observed in Cd(II) complexes with cyclens bearing four alcohol-containing pendant arms.[15,24,25] and in the simple DOTA-tetraamide.[16] An almost ideal C_4-symmetric TSA pattern was found in a Cd(II) complex of DOTA-tetrakis(propargylamide).[13,26,27] However, only two solid-state structures of Hg(II) complexes with cyclen-based ligands containing coordinating pendant arms have been described to date. The Hg(II) DOTA-tetraamide complex presents an unsymmetrical structure in which all eight donor atoms are bound in a pattern close to the TSA arrangement, with two oxygen donor atoms at a longer distance than the other two.[28] The recently determined structure of the [Hg(H₂dota)] complex exhibits an unsymmetrical [6 + 1] heptacoordination of the central ion. In this structure, two opposite, deprotonated acetate pendant arms are coordinated at a short distance and one of the two protonated acetic acid pendant arms is coordinated at a significantly longer distance. The fourth, uncoordinated, pendant

arm is oriented toward the central ion but at a non-bonding distance.[29]

Structural solution studies are even less frequent. The solution fluxionality of Cd(II) and Hg(II) complexes of tetrakis[(2-methyloxy)ethyl]-cyclen was observed and it was interpreted as interchange of the pendant arm helicity of the TSA geometry around the metal ions.[30] The fluxionality of the Cd(II) complex of symmetric tetrakis(methylpyrazol)-substituted cyclen was explained by the inversion of the four five-membered chelate rings formed by coordination of the Cd(II) ion by ethylene-diamines of cyclen.[27] The same effect was also observed for the Cd(II) complex of the related bis(methylpyrazol)–bis(carboxymethyl) substituted cyclen.[31] The fluxionality of the coordination sphere has also been demonstrated by ^{13}C NMR for Zn(II) and Cd(II) complexes of symmetric tetrakis(hydroxypropyl) cyclen.[15]

Surprisingly, only a handful of complexes of the parent ligand, DOTA, with divalent metal ions have been structurally characterized.[20,32–38] In the present work, we aim to fill the gap and to study complexes of DOTA with Group 12 metal ions, Zn(II), Cd(II) and Hg(II), in order to investigate the influence of the metal ion size and charged strongly bound carboxylate pendant arms on the structural properties of the complexes and to explore the possibilities of solid-state NMR spectroscopy (ss-NMR) to study the structures of such molecular complexes. This study thus aims to elucidate the structural and dynamic aspects of DOTA complexes with these divalent metal ions, specifically focusing on the coordination modes, flexibility, and fluxionality of pendant arms. Moreover, understanding these interactions and structural parameters will also contribute to developing methods for the characterization of structurally precise transition metal ion crosslinked biopolymers such as alginates and pectin which currently attract considerable attention in many fields of materials science.[39,40]

Results

Synthesis

Transition metal complexes in their protonated form [M(H₂dota)] where M = Zn, Cd, and Hg were prepared in aqueous solution by reaction of the zwitter-ionic form of DOTA with freshly prepared metal oxide/hydroxide to avoid the introduction of any anions into the solution. These neutral complexes were isolated as microcrystalline materials and have a relatively low solubility in water. They were used in the syntheses of complex salts. The obtained materials were not suitable for single-crystal X-ray diffraction analysis. However, single crystals of the [Cd(H₂dota)] complex were obtained by vapour diffusion of acetone into its diluted aqueous solution. The deprotonated complexes were synthesised by the addition of the respective alkali metal hydroxide just to neutralize two remaining acidic protons, either as a solid or as a saturated solution (Ba(II) hydroxide), to a suspension of the diprotonated complexes in water. The solids used for X-ray structural analysis were obtained by acetone vapour diffusion into aqueous solutions

of the deprotonated complexes. The same phases were also used for ss-NMR measurements. Preparation of other salts (Ca^{2+}, Sr^{2+}, K^+, Me_4N^+, *etc.*) was also attempted; however, only formation of oils or fine powders was observed.

Solid-state structures

Five compounds were prepared in a form suitable for single-crystal X-ray diffraction: $[Cd(H_2dota)]·H_2O$, $Ca[Hg(dota)]·9.5H_2O$, $Ba[Hg(dota)]·8.5H_2O$, $Ba[Cd(dota)]·12H_2O$ and $Ba[Zn(dota)]·5.5H_2O$. Experimental details concerning the X-ray diffraction studies are given in Table S1.

$[Cd(H_2dota)]·H_2O$ crystallised in a centrosymmetric monoclinic $P2_1/n$ space group. The asymmetric unit comprises one $[Cd(H_2dota)]$ complex molecule and one water molecule (Fig. 1). The Cd(II) ion is heptacoordinated by four cyclen amine nitrogen atoms and three oxygen atoms, two originating from deprotonated and one from protonated acetates in the pendant arms, respectively. The carbonyl oxygen atom of the protonated pendant arm is bound at a longer distance (2.766 Å) while the second protonated pendant arm remains at a non-bonding distance (3.096 Å), although its carbonyl oxygen atom is still oriented toward the central metal ion. The Cd(II) ion lies between almost parallel N_4 and O_4 planes, closer to the N_4 plane (the N_4 plane is defined by four coordinated cyclen amine nitrogen atoms and the O_4 plane is formed by three coordinated pendant oxygen atoms and the carbonyl oxygen atom of the non-bound acetic acid pendant arm). These planes are mutually twisted by approximately 26°. Therefore, we can view the coordination polyhedron as derived from a twisted square antiprism where one donor atom was removed. The parent "octacoordinated" structure has a Δ-δδδδ/Λ-λλλλ configuration. The crystal packing is stabilised by hydrogen bonds between the protonated and deprotonated pendant arms, and the water molecule.

$Ca[Hg(dota)]·9.5H_2O$ crystallised in a monoclinic $C2/c$ space group. The asymmetric unit comprises two crystallographically independent halves of two $[Hg(dota)]^{2-}$ complex anions, one Ca(II) cation and 9.5 water molecules of crystallization which are partially disordered (see the SI). The complex anions labelled "A" and "B" (Fig. 2 and Table S2) are generated by
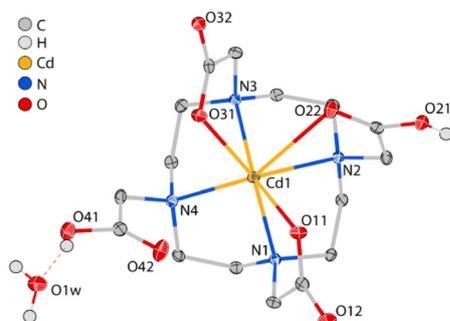

Fig. 1 Solid-state structure of $[Cd(H_2dota)]·H_2O$. Carbon-bound hydrogen atoms are omitted for clarity. Thermal ellipsoids are drawn at the 50% probability level.

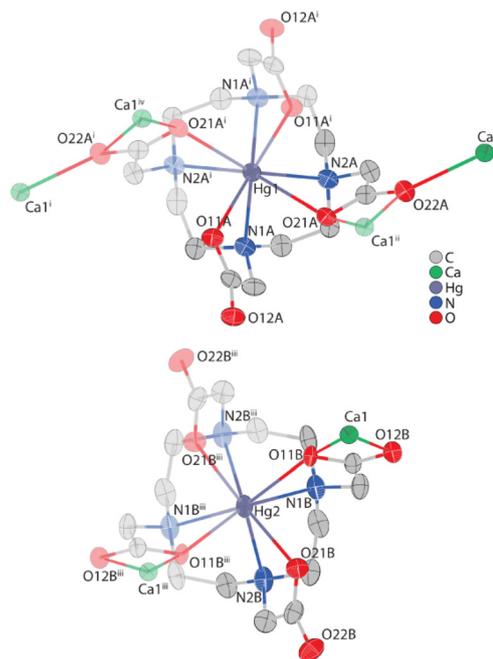**Fig. 2** Molecular structures of complex anions "A" (top) and "B" (bottom) found in the solid-state structure of $Ca[Hg(dota)]·9.5H_2O$. Hydrogen atoms are omitted for clarity. Thermal ellipsoids are drawn at the 50% probability level. Semi-transparent parts of the anions are generated by C_2 axes of symmetry or belong to the neighbouring asymmetric units (Ca(II) counter-ions). Symmetry codes: i: $1 - x$, y, $3/2 - z$, ii: $1 - x$, $1 - y$, $1 - z$, iii: $1 - x$, y, $1/2 - z$, and iv: x, $1 - y$, $1/2 + z$.

rotation around the C_2 symmetry axis running through the Hg(II) ions and perpendicular to the N_4 plane. The Hg(II) ion lies between parallel N_4 and O_4 planes closer to the N_4 plane. The planes are mutually twisted at about 25° and 22–23° in the molecules "A" and "B", respectively; thus, both ligand cages exhibit a distorted TSA arrangement. In anion "A", the Hg(II) ion is coordinated in an enantiomeric configuration Λ-λλλλ. The O–Hg–O angles 117.8° and 112.4° point to some difference between the coordinated oxygen atoms but the N–Hg–N angles (118.6° and 118.9°) and are more similar to each other. The Hg–N and Hg–O distances are 2.433/2.448 Å and 2.441/2.665 Å, respectively. Two oxygen atoms are located significantly farther away from the central metal ion due to their simultaneous coordination to the Ca(II) counter-cation. Thus, these two pendant acetate groups form a bridge between two crystallographically equivalent Ca(II) counter-cations and the central Hg(II) ion. The oxygen atom O21A binds simultaneously to one Ca(II) ion ($1 - x$, $1 - y$, $1 - z$) and the central Hg(II) ion in the μ^2-bridging mode while O22A coordinates two Ca(II) ions in a simple μ^2-bridging mode (one in the elementary cell position, the other Ca(II) cation is at position $1 - x$, $1 - y$, $1 - z$). Thus, one Ca(II) cation ($1 - x$, $1 - y$, $1 - z$) is coordinated by this acetate pendant arm in the κ^2-O,O' mode. The anion "B" is an opposite, Δ-δδδδ, enantiomer of the anion "A". The Hg(II) ion is coordinated significantly more regularly with Hg–N and Hg–O bond lengths of 2.466–2.484 Å and

2.560–2.573 Å, respectively. The difference in coordination geometries between these two complex anions can be attributed to the different modes of coordination to the Ca(II) counter-cation. In the complex anion "A", two acetate pendant groups are coordinated to two crystallographically equivalent Ca(II) and to the central Hg(II) ions. In contrast, in the complex anion "B", acetate pendant arms are bound to only one Ca(II) counter-cation in the κ^2-O,O' fashion (O11B is coordinated to Hg(II) and Ca(II) ions in the μ^2-bridging mode while O12B is coordinated to only one Ca(II)$^+$ ion). Therefore, it can be suggested that the counter-cations exert lesser influence on the structure of the complex anion "B". In both anions, only two of the four pendant arms interact with Ca(II) cations.

In both complex anions, half of the mercury-bound oxygen atoms also form a bridge to one or two Ca(II) counter-cations. The pendant carboxylates non-coordinated to the Ca(II) cation form multiple hydrogen bonds to water molecules of crystallization. All these interactions lead to a complicated 3D-structure; its more detailed description and the crystal packing discussion are given in the SI.

Ba[Hg(dota)]·8.5H$_2$O crystallised in a triclinic space group $P\bar{1}$. In the asymmetric unit, there are four crystallographically independent [Hg(dota)]$^{2-}$ complex anions, designated as A–D, four Ba(II) counter-cations (see Fig. 3) and 34 partially dis-

Fig. 3 Molecular structures of two of four complex anions ("A" – top; "D" – bottom) found in the solid-state structure of Ba[Hg(dota)]·8.5H$_2$O. Hydrogen atoms are omitted for clarity. Thermal ellipsoids are drawn at the 50% probability level. Symmetry codes: i: 1 − x, 2 − y, 1 − z; ii: 1 − x, 1 − y, 1 − z; iii: 2 − x, 1 − y, 1 − z; and iv: 2 − x, −y, −z.

ordered water molecules of crystallisation (see the SI for more information; Table S3 and Fig. S2). The central Hg(II) ion in all four complex anions is coordinated in a distorted TSA geometry (the Λ-λλλλ and Δ-δδδδ enantiomers are mutually related by crystallographic inversion) as further evidenced by the O–Q_O–Q_N–N torsion angles (from 20.7° to 30.3°; the ideal angle is 22.5°). The Hg(II) ion lies between these N$_4$ and O$_4$ planes, closer to the N$_4$ plane (Hg–Q_O 1.38–1.42 Å and Hg–Q_N 1.21–1.24 Å). The O–Hg–O angles range from 107.7° to 116.2° and the N–Hg–N angles range from 119.3° to 120.9°.

In anions "A" and "C", the central Hg(II) ion is coordinated in an octadentate 6 + 2 fashion with an approximate pseudo-C_2 symmetry by four nitrogen atoms (Hg–N bond lengths are 2.438–2.472 and 2.421–2.469 Å, respectively) and four oxygen atoms (Hg–O bond lengths are 2.437–2.648 and 2.462–2.652 Å, respectively) of the acetate pendant arms. Two coordinated oxygen atoms are always closer to the Hg(II) ion and the other two are in more distal positions. Four different Ba(II) counter-cations are coordinated by each macrocyclic anion, out of which two are from the neighbouring asymmetric unit. The Ba(II) cations from the same asymmetric unit are coordinated by only two oxygen atoms (O22A, O42A, O22C and O42C) of two carboxylate pendant arms with the shorter Hg–O bonds (~2.44 and ~2.46 Å for molecules "A" and "C", respectively) whereas the counter-cations from neighbouring asymmetric units are coordinated in a more complicated fashion. One of them is coordinated by two oxygen atoms (O41A, O42A and O21C, O22C) of one acetate pendant arm in a κ^2-O,O' fashion and the other one is coordinated by two oxygen atoms (O21A, O22A and O41C, O42C) of one acetate pendant arm and one (Hg-coordinated) oxygen atom of another acetate pendant arm (O31A and O11C) in a κ^3-O,O',O'' fashion. In contrast, two acetate pendant arms with longer Hg–O bonds (~2.64 and ~2.65 Å, respectively) also participate in hydrogen bonds with two/three different water molecules.

In anion "B", the central Hg(II) ion is coordinated in a 7 + 1 fashion by four nitrogen atoms (Hg–N bond lengths 2.413–2.461 Å) and three/four acetate oxygen atoms (Hg–O bond lengths 2.333–2.751). This anion contains three differently disordered acetate pendant arms (see the SI for details), one of which is disordered between the coordinated and uncoordinated modes; Hg–O distances for the coordinated and non-coordinated oxygen atoms are ~2.48 Å and ~2.97 Å, respectively. Two different Ba(II) counter-cations are coordinated by this complex anion, both originating from neighbouring asymmetric units. The Ba(II) cations are coordinated by two oxygen atoms (O11B, O12B and O21B, O22B) of one acetate pendant arm and one (Hg-coordinated) oxygen atom of another acetate pendant arm (O31B and O42B) in a κ^3-O,O',O'' fashion.

In the anion "D", the central Hg(II) ion is also coordinated in a 7 + 1 fashion by four nitrogen atoms (Hg–N bond lengths 2.419–2.467 Å) and four acetate oxygen atoms (Hg–O bond lengths 2.476–2.624 Å). Two different Ba(II) counter-cations are coordinated by this complex anion, both originating from neighbouring asymmetric units. One of them is coordinated
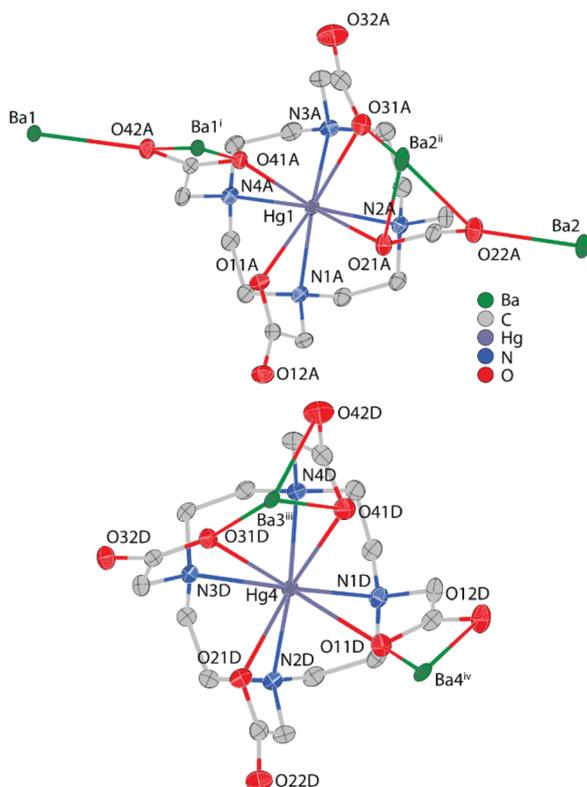
by two oxygen atoms of one acetate pendant arm (O11D, O12D) in a κ^2-*O,O′* fashion and another is coordinated by two oxygen atoms (O41D, O42D) of one acetate pendant arm and one (Hg-coordinated) oxygen atom of another acetate pendant arm (O31D) in a κ^3-*O,O′,O″* fashion.

All non-coordinated carboxylate oxygen atoms are connected to a network of water molecules of crystallisation through hydrogen bonds and the pendant arm oxygen atoms are acting as acceptors in the hydrogen bond network. These interactions lead to a complicated 3D structure; its more detailed description and the crystal packing are given in the SI.

Ba[Cd(dota)]·12H$_2$O crystallised in a triclinic $P\bar{1}$ space group. The asymmetric unit contains two crystallographically independent [Cd(dota)]$^{2-}$ complex anions labelled "A" and "B" (see Fig. 4), two Ba(II) counter-cations and 24 partially disordered water molecules of crystallization (see the SI for more information).

In both complex anions "A" and "B", the central Cd(II) ion is coordinated in an octadentate 6 + 2 fashion, derived from the TSA geometry with two longer Cd–O bonds. Both Cd(II) ions lie between the N$_4$ and O$_4$ planes, closer to the N$_4$ plane and the planes are mutually twisted by 23.7–26.0° (Table S4 and Fig. S3). The O–Cd–O "opening" angles are in range 111.1–117.4° while the N–Cd–N angles are mutually very similar (116.4–116.8°). The enantiomeric Δ-δδδδ/Λ-λλλλ

anions are related by crystallographic inversion. In the more symmetric anion "A", two opposite ("*trans*") Cd–O bonds are shorter (2.368 and 2.377 Å) while the other two "*trans*" Cd–O bonds are longer (2.508 and 2.519 Å) whereas two adjacent Cd–N bonds are shorter (twice 2.443 Å) and two other Cd–N bonds are longer (2.469 and 2.483 Å). In the less symmetric cation "B", the Cd–N distances are in the range 2.418–2.467 Å and, surprisingly, two adjacent ("*cis*") Cd–O bonds are shorter (2.384 and 2.430 Å) and other two "*cis*" Cd–O bonds are longer (2.457 and 2.495 Å). In both units, one pendant carboxylate is involved in hydrogen bond network and other three carboxylate groups are binding the Ba(II) counter-cations in various ways. Details and crystal packing are given in the SI.

Ba[Zn(dota)]·5.5H$_2$O crystallized in a monoclinic $P2_1/n$ space group. The asymmetric unit contains two crystallographically independent [Zn(dota)]$^{2-}$ complex anions "A" and "B" (Fig. 5), two Ba(II) counter-cations and eleven water molecules.

In the complex anion "A", the central Zn(II) ion is hexacoordinated in a distorted octahedral fashion by four nitrogen donor atoms and two oxygen donor atoms originating from two opposite ("*trans*") acetate pendant arms. The Zn–N bond lengths fall in the range 2.197–2.334 Å and the Zn–O bond lengths are 2.082 and 2.125 Å (Table S5). The closest oxygen atoms of the non-coordinated pendant arms are located at distances of 2.979 and 3.210 Å from the Zn(II) cation. Twist angles

Fig. 4 Molecular structures of anions "A" (top) and "B" (bottom) found in the solid-state structure of Ba[Cd(dota)]·12H$_2$O. Hydrogen atoms are omitted and only the major part of the disorder is shown for clarity. Thermal ellipsoids are drawn at the 50% probability level. Symmetry codes: i: −*x*, −*y*, 1 − *z*; ii: 1 − *x*, 1 − *y*, 1 − *z*.
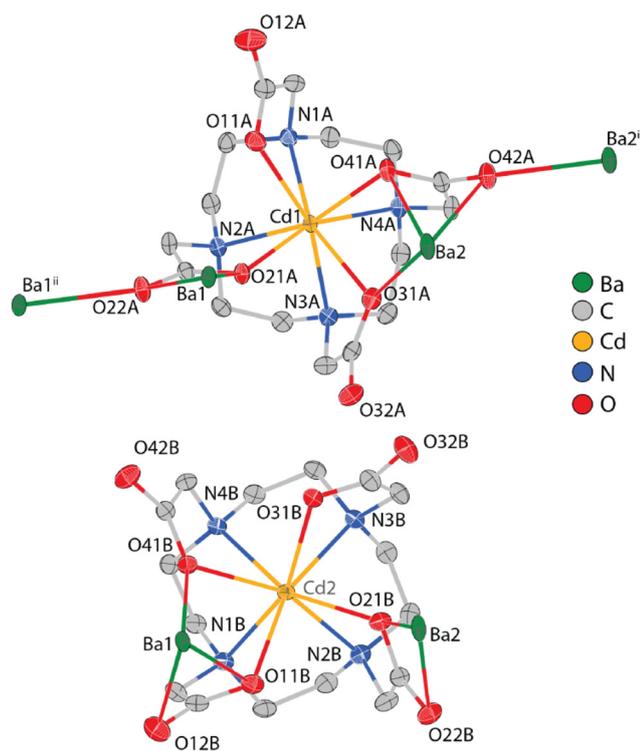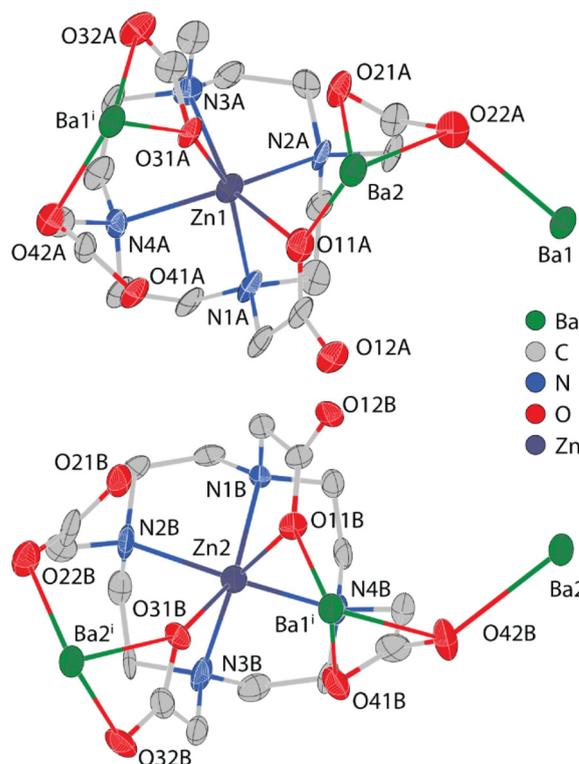

Fig. 5 Molecular structures of complex anions A (top) and B (bottom) found in the solid-state structure of Ba[Zn(dota)]·5.5H$_2$O. Hydrogen atoms are omitted for clarity. Thermal ellipsoids are drawn at the 50% probability level. Symmetry codes: i: *x* − 1, *y*, *z*.

N–Q_N–Q_{2O}–O (Q_N is a centroid of N atoms; Q_{2O} is a centroid of two coordinated O atoms) are ~27° which is similar to the values found in the corresponding TSA arrangements described above. The chirality of this anion is Δ-δδδδ. In the complex anion "B", the central Zn(II) ion is hexacoordinated analogously to anion "A". The Zn–N bond lengths range from 2.196 to 2.358 Å and Zn–O bond lengths are 2.048 and 2.138 Å. The closest oxygen atoms of the non-coordinated pendants are in distances of 3.015 Å and 3.207 Å from the Zn(II) ion. The arrangement is slightly closer to that of the ideal octahedron than that in anion "A" with the twist angles N–Q_N–Q_{2O}–O having values of 26.7–30.0°. The chirality of this anion is Λ-λλλλ. In both species, the O–Zn–O angle is close to the theoretical 90° (~88°). The intermolecular interactions and coordination around the Ba(II) counter-cation are similar in both complex anions "A" and "B" (Fig. S4). The Zn(II)-non-co-ordinated carboxylate groups are involved in interactions with the Ba(II) cations and/or in hydrogen bonds. These interactions lead to a complicated 3D structure and its more detailed description is given in the SI.

Solid-state NMR

Solid-state NMR (ss-NMR) measurements were carried out on bulk crystalline samples from which the single crystals used for X-ray diffraction analysis had been selected. To verify that the bulk material corresponded to the single crystalline phase, five to ten crystals from the particulate synthetic batch were examined by single-crystal X-ray diffraction and they all always yielded identical crystallographic parameters. These verified bulk samples were then immediately used for the ss-NMR measurements and treated as pure single-phase materials.

In their Ba(II) salts, the [M(dota)]$^{2-}$ complex anions exhibit different coordination modes which should also be reflected in the ss-NMR spectra. Thus, the prepared phases were characterised by ^{13}C and ^{15}N ss-NMR spectroscopy. Importantly, the number of crystallographically independent anions in the asymmetric unit varies among these phases and it directly influences an expected number of signals observed in their ss-NMR spectra. For example, Ba[Hg(dota)]·8.5H$_2$O with $Z = 4$ will theoretically produce $4 \times 16 = 64$ peaks in its ^{13}C ss-NMR spectrum originating from 16 non-equivalent carbon atoms in each of four complex anions. Thus, due to the high number of expected peaks and the substantial overlap of these resonances, the spectra were deconvoluted into the necessary number of generalized, predominantly Lorentzian-shaped, peaks (the parameter L/G was kept at a constant value of 0.8 for all peaks) and the results are shown in Tables S6–S8. The ^{13}C and ^{15}N CP-MAS ss-NMR spectra were analysed accordingly (Fig. 6 and 7). The number of nuclei represented by a peak was determined based on their integral intensity. In all spectra, the integral intensities were normalised in such a way that their sum was equal to the number of independent carbon atoms in a single complex anion, *i.e.* sixteen ^{13}C and four ^{15}N atoms. Thereafter, these intensities were multiplied by a coefficient to convert them to integer numbers; the coefficient corresponds to the number of formula units per the asymmetric unit (Z)
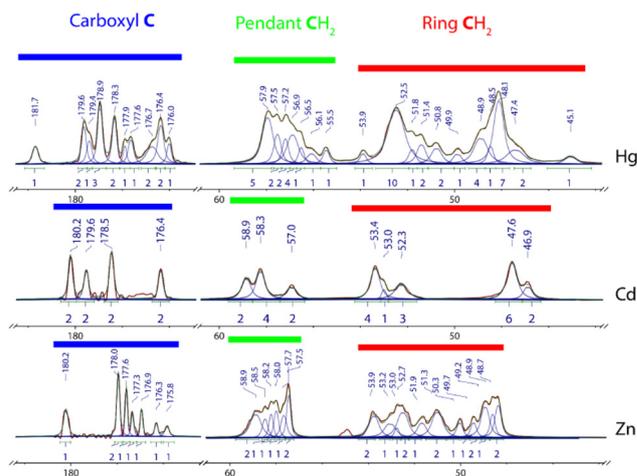

Fig. 6 The ^{13}C CP-MAS ss-NMR (126 MHz, 11 kHz) spectra of Ba(II) salts of Hg(II) (top), Cd(II) (middle) and Zn(II) (bottom) complexes. Relative integral intensities are rounded off to an integer number for simplicity; the complete line fitting analysis is given in the SI. Colour codes: maroon – experimental spectra, blue – resonances of individual sites, and green – sum of the resonances of the individual sites. Coloured bars represent the tentative assignment of the ^{13}C NMR signals to three different site types, according to the chemical shifts of the relevant carbon atoms in the solution spectra.
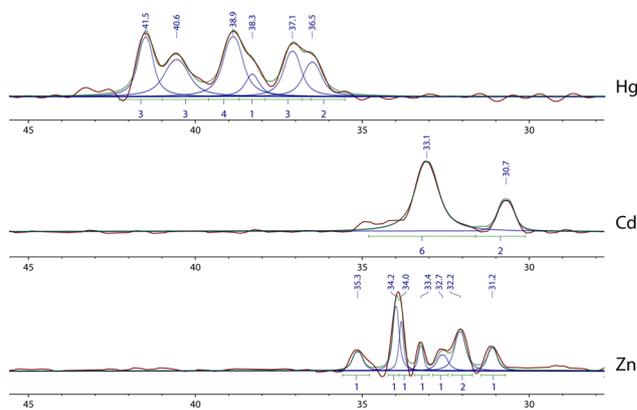
Fig. 7 The ^{15}N CP-MAS ss-NMR (71 MHz, 10 kHz) spectra of Ba(II) salts of Hg(II) (top), Cd(II) (middle) and Zn(II) (bottom) complexes. Relative integral intensities are rounded to an integer number for simplicity; the complete line fitting analysis is given in the SI. Colour codes: maroon – experimental spectra, blue – resonances of individual sites, and green – sum of the resonances of the individual sites.

determined by X-ray crystallography. For the ^{13}C ss-NMR spectra, it was 2 and 4 for the Zn(II)/Cd(II) and Hg(II) complexes, respectively. An analogous approach was used to fit the ^{15}N ss-NMR spectra of these three compounds, although the accidental overlap of ^{15}N resonances in the Cd(II) complex (Fig. 6) caused that the spectrum could also be consistent with $Z = 1$. It is noteworthy that the ss-NMR shifts of all nitrogen atoms in the Hg(II) complex are significantly higher than those in the complexes of the lighter metal ions (Tables S9–S11). This effect can be attributed to the relativistic spin–orbit effect

of the central Hg(II) ion on the directly bound nitrogen atoms.[41] Although the Cd(II) and Zn(II) complexes have the same number of distinct anions in the asymmetric unit, there is a different number of resolved peaks in their respective ^{13}C ss-NMR spectra. This is especially evident in the pendant CH$_2$ and ring CH$_2$ signals in the methylene region of the ^{13}C ss-NMR spectra. In the spectrum of the Zn(II) complex, the peaks represent at most two different nuclei, whereas in the spectrum of the Cd(II) complex, the peaks represent up to six different nuclei.

Solution dynamics

For complexes of DOTA with divalent metal ions, no information about solution dynamics are available, except mutual exchange of enantiomers observed in the [Hg(dota)]$^{2-}$ complex; however, no thermodynamic parameters have been given.[29] Thus, the solution dynamics of the title complexes was investigated here using variable-temperature (VT) ^{13}C{^{1}H} NMR spectroscopy. Since only one ^{13}C NMR signal (and one [113]Cd or [199]Hg NMR signals, see Fig. S9 and S10) was observed for the carboxyl groups as well as for the pendant and ring methylene carbon atoms at ambient temperature, the complexes are fully fluxional. These ^{13}C nuclei are therefore in a rapid exchange and they are equivalent on the NMR time scale. To observe any molecular dynamics, the measurements had to be conducted at low temperatures, even below the water freezing point. Therefore, the complexes were dissolved in a D$_2$O/CD$_3$OD mixture to lower the freezing point of the solutions. In the temperature range used, coalescence of two ^{13}C NMR signals assigned to the macrocyclic carbon atoms was observed at temperatures approximately −30, +20 and +10 °C for the Zn(II), Cd(II) and Hg(II) complexes, respectively. Below this temperature, two peaks were observed for the macrocyclic ring methylene carbons, but one signal remains for the carboxyl and pendant methylene carbon atoms, and the same behaviour was observed for each studied complex. The ^{13}C{^{1}H} VT NMR spectra are shown in the SI (Fig. S5–S7). Fitting of the VT ^{13}C NMR data gave thermodynamic parameters of the exchange process. Unfortunately, only one spectrum of the [Zn(dota)]$^{2-}$ complex below the coalescence temperature could be collected and it precludes a definitive determination of separation of the exchanging peaks. To assess the dynamics of these systems quantitatively, the rate constants k_{ex} of the interconversion between the exchanging species were calculated for temperatures below and above the coalescence using eqn (1) and (2), respectively.

$$k_{ex} = \pi(w - w_0) \tag{1}$$

$$k_{ex} = \frac{\pi \Delta \nu^2}{2(w - w_0)} \tag{2}$$

Here, w denotes full width at half-maximum (FWHM) of the exchanging signal, w_0 is the FWHM of a non-exchanging signal (the carbonyl ^{13}C NMR signal was used as it remains in the fast regime throughout the used temperature range) and $\Delta \nu$ represents the chemical shift difference (in Hz) between the exchanging signals. Eyring plots (Fig. 8) were constructed from the VT data and the experimental rate constants k_{ex} were fitted by a linear function to obtain the activation parameters. The analysis yielded positive activation enthalpies for all three complexes (Table 1), in agreement with the negative slopes observed in the Eyring plots. The estimated values are about +35, +61, and +54 kJ mol^{-1} for the Zn(II), Cd(II), and Hg(II) complexes, respectively.

Discussion

Four new salts of three DOTA complexes were prepared and studied in the solid state, Ca[Hg(dota)]·9.5H$_2$O, Ba[Hg(dota)]·8.5H$_2$O, Ba[Cd(dota)]·12H$_2$O and Ba[Zn(dota)]·5.5H$_2$O. These compounds were chosen, as for divalent d^{10} metal ions Zn(II), Cd(II) and Hg(II), mainly the size of the ions should influence the properties of their complexes with DOTA, as the most "classical" ligand among cyclen derivatives. Their molecular structures in the solid state were determined by single-crystal X-ray diffraction. Trends in structural parameters can be compared with those in complexes of analogous cyclen derivatives.

The smallest member of the series, Zn(II) ions, prefers an octahedral coordination environment. Both independent Zn(II) complex cations exhibit the same N$_4$O$_2$ octahedral arrange-
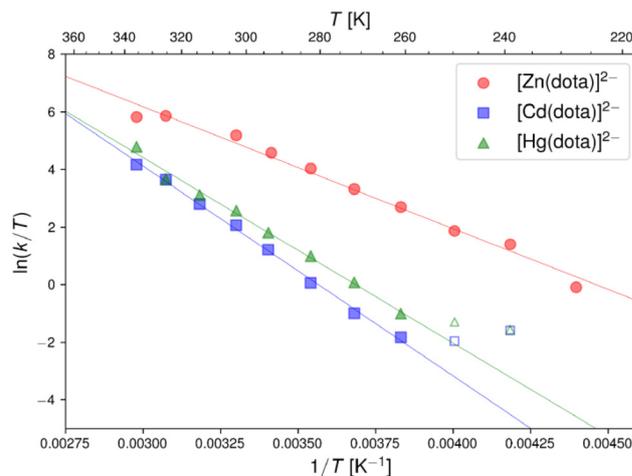
Fig. 8 Eyring plots for interconversion of two ring carbon ^{13}C NMR signals. The empty symbols represent values which significantly deviate from the linear trend and were not used for linear regression.

Table 1 Activation parameters for the macrocycle chelate ring interconversion of the [Zn(dota)]$^{2-}$, [Cd(dota)]$^{2-}$ and [Hg(dota)]$^{2-}$ complexes in D$_2$O/CD$_3$OD solutions

Compound	$\Delta H^{\ddagger}$ (kJ mol^{-1})	$\Delta S^{\ddagger}$ (J K^{-1} mol^{-1})	$^{298}\Delta G^{\ddagger}$ (kJ mol^{-1})
[Zn(dota)]$^{2-}$	+37.0 ± 1.2	−33 ± 4	+47.0 ± 1.8
[Cd(dota)]$^{2-}$	+60.6 ± 1.3	+18 ± 4	+55.1 ± 1.8
[Hg(dota)]$^{2-}$	+53.6 ± 1.7	−0.1 ± 6	+54 ± 2

ment with two non-coordinated pendant acetates and differences between them are not significant. This coordination mode is similar, albeit significantly more distorted if compared to that found in the previously published structure of the diprotonated form of the complex.[20,33] In the present fully deprotonated anion, distance between the Zn(II) ion and the uncoordinated pendant oxygen atom is significantly smaller than that in the diprotonated form (2.978–3.210 Å *vs.* 5.307 Å, respectively). This difference is caused by different intermolecular interactions stabilising structures of each form of the complex. In the diprotonated form, the structure is stabilised by a network of hydrogen bonds between protonated noncoordinated carboxylate pendant arms and coordinated oxygen atoms of the neighbouring complex unit. On the other hand, structure of the Ba(II) salt of the $[\text{Zn}(\text{dota})]^{2-}$ anion is stabilised by coordination of the pendant arms to the Ba(II) counter-cations. Since the same Ba(II) cation coordinates oxygen atoms of both Zn-coordinated and Zn-non-coordinated pendant arms, the Zn-non-coordinated pendant arms are forced to be closer to the Zn(II) ion instead of being stretched out, as was found in the structure of the diprotonated complex. In contrast to $\text{Ba}[\text{Zn}(\text{dota})]\cdot5.5\text{H}_2\text{O}$, the Zn(II) ion in several of the published structures of complexes of cyclen-based ligands is in a more regular octahedral coordination characterised by small ($<10°$) $\text{N}–\text{Q}_\text{N}–\text{Q}_{2\text{O}}–\text{O}$ torsion angles.[15,20] The Zn(II) ion in the present structure is coordinated more akin to coordination modes in Zn(II) complexes of other macrocyclic ligands[13,14,16,42] where torsion $\text{N}–\text{Q}_\text{N}–\text{Q}_{2\text{O}}–\text{O}$ angles in the range 20–30° were observed as well. This indicates that the octahedron is significantly distorted to a trigonal prism and these structures are seemingly derived from the TSA geometry by removal of two opposite donor atoms from the O_4 plane. Nonetheless in several structures, the non-coordinated pendant arms are oriented in such a way that potential donor atoms are directed towards the central metal ion but in a non-bonding distance. In the structures of other divalent first-row transition metal ion complexes of the diprotonated DOTA, small $\text{N}–\text{Q}_\text{N}–\text{Q}_{2\text{O}}–\text{O}$ torsion angles ($<10°$) were observed,[20,32,33,37] except for the Mn(II) complex ($\sim26°$).[35,36] This difference is caused by different orientations of non-coordinated pendant arms. This orientation can be either away from the metal ion (low torsion angles) or towards the metal ion (higher torsion angles, present in the title complex).

In contrast to the Zn(II) ion, the larger metal ions of the series can accommodate more donor atoms. The Cd(II) ion in the structure of the barium(II) salt was observed in two distinct $[6 + 2]$ coordination environments where four macrocycle amine nitrogen atoms are bound with similar Cd–N bond distances forming a N_4 plane but two pendant arms interact with the central metal ion more strongly than the other two (Fig. 4). In one complex anion, two longer Cd–O bonds originate from two opposite ("*trans*") pendants. The Cd(II) complex of the DOTA-tetraamide (DOTAM, Fig. 9) adopts a similar $[6 + 2]$ TSA-derived geometry but difference between the short and long Cd–O distances is more pronounced.[16] In the other complex anion, oxygen atoms with two longer Cd–O bonds belong, sur-
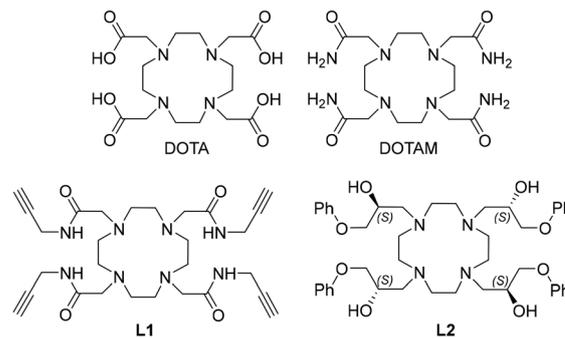

Fig. 9 Formulae of the discussed ligands.

prisingly, to two adjacent ("*cis*") pendants. This difference in the geometry of the coordination polyhedra is mainly caused by the different coordination of the Ba(II) counter-cations by the pendant arms. On the other hand, Cd(II) ions have also been observed in almost regular TSA coordination polyhedra in structures of Cd(II) complexes of DOTA-tetrakis(propargylamide) (**L1**, Fig. 9) and 1,4,7,10-tetrakis[(S)-2-hydroxy-3-phenoxy-propyl]-cyclen (**L2**, Fig. 9).[13,26] The $\text{N}–\text{Q}_\text{N}–\text{Q}_\text{O}–\text{O}$ torsion angles in the published structures range from 11.6° to 25.6°, clearly demonstrating the preference of Cd(II) complexes of cyclen-based ligands bearing four coordinating pendant arms for the TSA geometry.[13,15,16,24–27,43,44] These structures can be classified according to the distances of the pendant donor atoms to the Cd(II) ion in a $[6 + 2]$ fashion[15,16,25,41] (6 examples) and $[7 + 1]$ fashion[15,24,26,31,41,42] (6 examples) and close to the regular octacoordination[13,26] (three examples).

The easy change of strongly bound pendant acetates in "*trans*" and "*cis*" positions suggests that such a change in the coordination of the pendant arms is also possible in solution (see below). In the structure of the protonated complex $[\text{Cd}(\text{H}_2\text{dota})]\cdot\text{H}_2\text{O}$, the Cd(II) ion is coordinated in a $6 + 1$ fashion. This structure is isostructural with the published structure of the diprotonated Hg(II) complex, $[\text{Hg}(\text{H}_2\text{dota})]\cdot\text{H}_2\text{O}$.[29]

Two phases with Hg(II) ions and Ca(II) and Ba(II) counter-cations were crystallized. In these compounds, complex units contain Hg(II) ion in polyhedra with CN 6–8. All geometries of the Hg(II) complexes can be considered to be derived from the TSA arrangement by elongation of one or more Hg–O bonds and with the N_4 plane well defined. In the solid-state structure of $\text{Ca}[\text{Hg}(\text{dota})]\cdot9.5\text{H}_2\text{O}$, the geometry of the two complex units differs. The first anion shows remarkable differences in lengths of two pairs of opposite Hg–O bonds, indicating the $[6 + 2]$ coordination mode. In contrast, the second anion shows almost identical bond lengths for all Hg–O bonds. This is caused by a different number of Ca(II) counter-cations coordinated to the acetate pendant arms in each complex unit. In the solid-state structure of $\text{Ba}[\text{Hg}(\text{dota})]\cdot8.5\text{H}_2\text{O}$, the $[6 + 2]$, disordered $[7 + 1]/[6 + 1]$, and $[7 + 1]$ coordination environments were found. The variability of the coordination polyhedra is caused not only by the different coordination of the Ba(II) counter-cations and other intermolecular interactions

such as hydrogen bonding but also by a much greater stereo-chemical capability of the Hg(II) cation itself. In the recently published structure of the protonated [Hg(H$_2$dota)] complex,[29] the Hg(II) ion was found in a [6 + 1] highly distorted coordination environment. The fourth pendant arm remained uncoordinated and is engaged in hydrogen bonding with a water molecule of crystallisation. On the other hand, the Hg(II) ion in the solid-state structure of the [Hg(dotam)]$^{2+}$ cation is octa-coordinated in the [6 + 2] fashion; structural parameters of this cation are very similar to the title complex.[16] These structures of the Hg(II) complexes demonstrate a high variability of the coordination modes available for the Hg(II) ion even if the ion is coordinated by closely related ligands, see Table 2.

All studied complexes share the same mutual combination of the conformation of the macrocycle chelate rings and the pendant arm "rotations", and the corresponding torsion angles are all below 30°. Thus, their geometry could be best described as the arrangement derived from the twisted square-antiprismatic (TSA) geometry. To see the differences in the coordination environments of the complex anions, the respective N–Q$_N$–Q$_O$–O torsion angles can be compared (Table 3). As the metal ion size increases, the average torsion angle decreases. It is consistent with general trends already observed

in lanthanide(III) complexes of DOTA and DOTA-like ligands where larger Ln(III) ions induce the decrease of the torsion angle.[12,45,46] Moreover, deviations in the angle are the smallest for the Cd(II) complex suggesting a lesser fluxionality of the Cd(II) complex anion. The high variability of torsion angles in the Hg(II) complex anions can be explained by a diversity of the coordination environments present in the studied solid-state structures. The position of the metal ion between the N$_4$ and O$_4$ planes follows the inverted trend to the torsion angles. Similarly, the "opening angle" (i.e. O–M–O bond angle) grows from the Zn(II) complex to the Cd(II) complex and then slightly falls for the Hg(II) complex (Table 3). Both parameters indicate a more "open" DOTA ligand cavity with Cd(II) and Hg(II) ions. However, these values (~105–116°) are significantly smaller than the "opening angles" in the TSA isomers of the Ln(III)–DOTA complexes (~122–126°)[45,46] and it indicates a more compact wrapping of these transition metal ions by DOTA if compared with Ln(III) ions. The same trends for the position of the metal ion with respect to the centroids of the N$_4$ and O$_4$/O$_2$ planes and for O–M–O opening angles were observed for the protonated [M(H$_2$dota)] (M = Zn(II), Cd(II) and Hg(II)) complexes (Table 3).

In the structures of the Ba(II) salts, there is an interesting coordination pattern of the Ba(II) cations which are co-

Table 2 Comparison of the structural parameters of Hg(II) complexes of H$_4$dota (Ca(II)/Ba(II) salts and their diprotonated form) and its tetraamide

Parameter	Ca–salt (A)	Ca–salt (B)	Ba–salt (A)	Ba–salt (B)	Ba–salt (C)	Ba–salt (D)	[Hg(H$_2$dota)][29]	[Hg(dotam)](ClO$_4$)$_2$ [28]
Distances, Å								
Hg–O	2.441	2.559	2.436	2.456	2.461	2.475	2.301	2.391
	2.441	2.559	2.487	2.476	2.529	2.531	2.425	2.434
	2.665	2.571	2.642	2.567	2.598	2.566	2.926	2.735
	2.665	2.571	2.649	2.751	2.653	2.624	3.221	2.815
Hg–N	2.433	2.466	2.439	2.413	2.421	2.418	2.387	2.414
	2.433	2.466	2.445	2.418	2.452	2.459	2.398	2.432
	2.448	2.484	2.465	2.447	2.466	2.461	2.479	2.453
	2.448	2.484	2.474	2.460	2.469	2.465	2.497	2.468
Angles, °								
O–Hg–O	112.36	115.79	107.69	111.33	109.35	114.00	105.36	107.4
	117.79	116.22	116.21	114.17	115.44	115.21	129.73	121.7
N–Q$_N$–Q$_O$–O^{a,b}	−25.98	22.11	−20.69	−24.37	−21.52	−23.71	−23.59	23.45
	−25.98	22.11	−21.09	−26.35	−21.96	−24.14	−23.89	23.98
	−26.06	23.21	−22.50	−26.41	−22.56	−24.50	−26.27	24.18
	−26.06	23.21	−22.83	−27.87	−24.08	−25.32	−27.60	26.47

^{a} Torsion angle. ^{b} The Q$_N$ and Q$_O$ are centroids of the N$_4$ and O$_4$ planes, respectively.

Table 3 Comparison of selected structural parameters in the studied complexes. Data for several independent complex units found in the solid-state structures are averaged and absolute values of the torsion angles are given (distances are in Å and angles in °)

Parameter^a	(dota)$^{4-}$			dotam			(H$_2$dota)$^{2-}$		
	Zn(II)	Cd(II)	Hg(II)	Zn(II)[16]	Cd(II)[16]	Hg(II)[28]	Zn(II)[20]	Cd(II)	Hg(II)[29]
N–Q$_N$–Q$_O$–O^b	28.30 ± 1.36	24.28 ± 0.99	23.86 ± 1.95	25.75 ± 4.04	24.41 ± 0.74	24.18 ± 1.16	7.07	26.03 ± 2.20	25.55 ± 0.66
M–Q$_N$	1.009 ± 0.007	1.290 ± 0.005	1.241 ± 0.024	0.946	1.263	1.220	0.891	1.239	1.219
M–Q$_O$	1.509 ± 0.002	1.318 ± 0.007	1.395 ± 0.028	1.558	1.319	1.389	1.444	1.339	1.433
O–M–O^c	88.1 ± 0.4	115 ± 2.28	114 ± 2.91	84.24	115.6 ± 5.9	114.6 ± 7.2	89.7	106.1	105.4

^{a} The Q$_N$ and Q$_O$ represent centroids of the N$_4$ and O$_4$ planes (Cd(II) and Hg(II) complexes), respectively, or centroids of the N$_4$ plane and two co-ordinated O atoms (for Zn(II) complexes), respectively. ^{b} Torsion angle. ^{c} "Opening" angle.

ordinated κ^2-*O,O'*-bidentately by both oxygen atoms of one acetate pendant arm and by an oxygen atom of the neighbouring acetate pendant arm. This interaction influences the coordination polyhedron of the central metal atom, and its effect can be seen primarily in the structure of the Cd(II) complex. Due to the smaller size of the Ca(II) cation, this type of interaction was not observed in the structure of Ca[Hg(dota)]·9.5H$_2$O as there is no space for such a coordination mode for the smaller metal ion. Comparing the structures of complexes of cyclen-based ligands with acetates or with other pendant arms, the acetate pendants interact with counter-ions relatively strongly and the interaction significantly influences their binding to the central metal ions, leading to a range of coordination modes in the solid state.

Fluxionality of the complex anions in solution was studied by VT ^{13}C NMR. All complexes displayed identical behaviour. At the low-temperature limit, single peaks were observed for each kind of carbon atoms (*i.e.* two for the pendant methylene/carbonyl resonances, and two for the ring carbon atoms). This suggests that, over the entire temperature range (from −40 to 60 °C), all four pendant arms are "equivalent" on the NMR time scale and their coordination is averaged by dynamics. This can be caused either by a symmetrical coordination of the pendants in solution or, more likely, by a rapid exchange due to their (weak) coordination/de-coordination. The dynamics results in the averaged ^{13}C NMR chemical shifts of carbon atoms in the pendant arms but still keeping the "effective" TSA arrangement of the entire complex species. Consistently with the variation of the CNs observed in the solid state, the process is probably "associative" (transiently increasing the CN, entropically unfavourable) for the Zn(II) complex and "dissociative" (transiently lowering CN) for the Cd(II) and Hg(II) complexes. Two distinct resonances of the ring carbon atoms point to an effective C_4 symmetry of the macrocyclic part and a frozen conformation of the chelate rings. Upon heating, resonances of the ring carbon atoms merged into one sharp peak in the high-temperature limit. In contrast, no significant change occurred for the pendant methylene signal and only a small change (~1 ppm upfield) was observed for the carbonyl resonances. The dynamics of the macrocycle ethylene chains is connected with mutual exchange between the TSA enantiomers.

Analogous dynamics have been observed for complexes of these divalent metal ions with several DOTA-like macrocyclic ligands where only the TSA arrangement and the averaging of only the pendant arms' NMR signals were observed. As the measurements were carried out in different solvents, a direct comparison of the current and the published data cannot be easily done. Although exchange parameters were not always provided, all complexes exhibit similar behaviour. Among Zn(II) complexes, the dynamics was followed only for Zn(II)–DOTAM in DMF and was proven to be very fast.[16] Several Cd(II) complexes of cyclen derivatives bearing alcohol[15,30] or pyrazol-1-ylmethyl[27,31] pendant arms have a similar coalescence temperature as the complex studied here. The Hg(II) complexes of DOTA,[29] DOTAM,[16] cyclen bearing alcohol[30] or

pyrazol-1-yl-methyl[31] pendant arms were also subjected to the ^{13}C VT-NMR study. A full analysis of our ^{13}C VT-NMR spectra provided energy barriers for the isomerisation process. The values indicate that the Zn(II) complex is the most fluxional one whereas the Cd(II) complex is the least fluxional. As the Zn(II) complex exhibits rather spread Zn–N distances (compared to more regular bond lengths in the Cd(II)/Hg(II) complexes) in the solid state (Table S6), the strength of the Zn(II)-amine group interaction in solution can be quickly altered and it could facilitate the ring interconversion. Values of the activation parameters are in agreement with data for complexes of other similar ligands.[16,30] A similar dynamic process in the TSA isomers was also observed for the Pb(II)–, Bi(III)– and Tl(III)–DOTA complexes and their kinetic parameters for the process are similar to those observed here for the Cd(II) and Hg(II) complexes.[47–49] The observed activation parameters are also similar to those for the TSA–SA exchange in the Ln(III)–DOTA complexes with CN 8/9.[50]

In NMR crystallography, precise determination of ^{13}C and ^{15}N chemical shifts plays a crucial role. Currently, the ss-NMR data are often combined with computational methods to determine the structures of crystalline and semi-crystalline materials at the atomic level. The distinct ^{13}C and ^{15}N chemical shifts can serve as reference parameters to validate crystal structures predicted by density functional theory (DFT) calculations. By comparing experimental and computationally derived NMR parameters, the most likely structural model can be identified. However, due to the high number of atoms (particularly heavy metal atoms) in the unit cell, combining ss-NMR spectroscopy with DFT calculations is not feasible in this study.

Nonetheless, if high-quality single-crystal X-ray data are absent, partial information about the solid-state structure remains valuable. This study demonstrates that ss-NMR spectroscopy can be an effective tool in such cases. ^{13}C ss-NMR spectroscopy unequivocally allowed to determine a number of non-equivalent complex species in the crystallographic unit cell and their crystallographic symmetry (C_1). Knowledge of the number of molecules in the asymmetric unit allows the determination of the correct space-group or the localization of molecules at special positions. This information could facilitate a successful structure solution from more readily obtainable powder X-ray diffraction data.[51] On the other hand, the ^{15}N ss-NMR spectroscopy produced erroneous results for the Cd(II) complex due to the resonance overlap. This significant overlap, observed in both ^{13}C and ^{15}N ss-NMR spectra of the Cd(II) complex, is likely caused by its more regular geometry compared to other complexes (see Table 3). This difference is most notable while comparing data for the Zn(II) complex. Despite having the same number of non-equivalent carbon/nitrogen atoms (as indicated by X-ray structures), the Zn(II) and Cd(II) complexes exhibit markedly different spectra. This contrast can be attributed to the lower symmetry of the Zn(II) complex where two Zn-coordinated pendants differ significantly from the other two. This also influences the geometry of the macrocyclic ring (compare the M–N bond length ranges for

the Zn(II) and Cd(II) complexes, Tables S5 and S6). On the other hand, the Cd(II) complex anions have a symmetry closer to C_4 symmetry, leading to smaller differences in the chemical environment of the nuclei. As a result, the individual methylene carbon atoms are mutually less different and are present as broadened resonances instead of multiple individual peaks.

ss-NMR spectroscopy has also proven to be a powerful tool to characterize local atomic environments in complex crystalline and semi-crystalline solids.[52] Our data provide insights into the influence of an identical counter-ion on the ^{13}C CP/ MAS ss-NMR spectra of Hg(II)-, Cd(II)-, and Zn(II)–DOTA complexes. The significant chemical shift variations (4–6 ppm) in the carbonyl regions are connected with differences in electron density and/or, more probably, in molecular interactions of the pendant arms. In these structures, coordination of the pendant arms to the Ba(II) counter-cations and involvement of the carboxylates in hydrogen bonds lead to noticeable differences in the chemical shifts; both kinds of interactions are expected to shift the carbonyl resonances downfield.[53,54]

Based on the analysis of connectivity of the pendant arms (Tables S17–S19), the carboxylate groups can be tentatively classified according to their intermolecular interactions. For the Zn(II) complex, six different interaction modes were identified. If all coordination bonds and all hydrogen bonds would affect the chemical shift of the carboxylate carbon atom in the same way, six resonances of carboxylate group would be expected in ^{13}C NMR spectra; a higher downfield shift would be expected with an increasing number of these interactions. However, the Castep DFT calculations (Table S16) showed that such assumption holds only for the Zn(II)-coordinated carboxylate carbon atoms which exhibit a lower calculated shielding than their Zn(II)-non-coordinated counterparts. Among the Zn(II)-coordinated carboxylates, resonances of carbon atoms of carboxylates involved in a bidentate interactions with the single Ba(II) counter-cations are more deshielded than those coordinating the single Ba(II) cation monodentately. Among the Zn(II)-non-coordinated carboxylate carbon atoms, those of carboxylates forming three coordination bonds to the Ba(II) counter-cations are shifted upfield relative to those forming only one coordination bond to the Ba(II) counter-cations but simultaneously engaged in one or two hydrogen bonds.

In the case of the Cd(II) complex, all pendant arms are coordinated to the Cd(II) ions and form no and up to three coordination bonds to the Ba(II) counter-cations. Hydrogen bonding further increases the total number of intermolecular interactions per carboxylate group to four or five. Assuming hydrogen bonds are less influential than coordination to the Ba(II) counter-cations, four peaks are expected in the spectrum; it is consistent with the experimental results.

The Hg(II) complex presents the most complicated case due to the high number of non-equivalent species in the unit cell. In this case, patterns analogical to those for the complexes of the lighter metal ions could not be identified. Nevertheless, the most notable resonance in the ^{13}C ss-NMR spectra is a high-frequency signal at *ca.* 182 ppm which is significantly shifted downfield from signals of all other carboxylate carbon atoms. This pronounced deshielding indicates a highly electron-deficient environment and can be tentatively assigned to carbon C42C. The respective carboxylate group is unique. It forms four coordination bonds (one to Hg(II) and three to two different Ba(II) ions) and participates in one hydrogen bond as an acceptor; thus, it can be expected to be the most deshielded carbon atom in the structure.

Conclusions and future perspectives

In this work, we studied complexes of DOTA with three d^{10} metal ions. The properties of these complexes should be determined primarily by the size of the metal ions. The X-ray diffraction studies revealed that the Zn(II) complex ion is hexacoordinated in a distorted octahedron with two bound pendant arms being in a mutual "trans" position, analogous to previous data on complexes of similar ligands. The Cd(II) and Hg(II) complex ions present (pseudo)octacoordinated structures with two pendant arms bound more strongly than the others. However, there is no strong evidence indicating which location of the pendant arms on the macrocycle is preferred for the stronger metal ion coordination. The structures are assigned to the twisted square-antiprismatic arrangement of the donor atoms, consistently with the large size of the metal ions. In the solution, all complexes are highly fluxional, showing a slow exchange of the ethylene chain of the macrocycle only at the lowest employed temperatures. The complexes exhibit full pendant arm equivalence. Consequently, we suggest that the pendant arms undergo very fast coordination and de-coordination, consistent with the easy change of the coordination numbers in the solid state. The fluxionality of these complexes is much higher than that in the Ln(III)–DOTA complexes.

The systematic changes in the ^{13}C and ^{15}N chemical shifts provide detailed insights into the electron density and coordination environment of the metal centres. The pronounced effects observed for the Hg(II) complex highlight the significant role of relativistic effects and covalent bonding on the ss-NMR data. These findings demonstrate the potential of ss-NMR not only as a characterization method but also as a powerful complement to diffraction techniques in NMR crystallography, enabling structural elucidation of phases where traditional methods face limitations. The number of individual resonances seems to correlate with the approximate symmetry of the complex anions. Furthermore, the ^{13}C NMR chemical shifts of the carboxylate carbon atoms were found to be dependent on the intermolecular interactions. This behaviour could further facilitate the structural elucidation in cases where good-quality single-crystal X-ray data are unavailable.

However, while the combined X-ray crystallography and ss-NMR approach presented here provides a detailed picture of coordination in the Zn(II)–, Cd(II)– and Hg(II)–DOTA complexes, several limitations should be acknowledged. Peak crowding, which is most critical for the Cd(II) complex, limited complete site-specific ^{13}C/^{15}N assignments and precluded extraction of NMR parameters that could strengthen structure–chemical

shift correlations. First-principles GIPAW–PBE benchmarking was carried out only for the Zn(II) phase, leaving relativistic effects in the Cd(II) and Hg(II) systems non-quantified, and molecular dynamics were assessed solely in solution, without complementary variable-temperature or relaxation measurements in the solid state. Future work should therefore be extended to GIPAW–DFT calculations and, where feasible, expand ^{113}Cd and ^{199}Hg NMR experiments to capture heavy-atom and covalency effects on NMR parameters: (i) it can deploy fast-MAS or DNP-enhanced multidimensional ss-NMR to resolve congested spectra and obtain full chemical-shift tensors and (ii) combine powder X-ray diffraction with NMR crystallography to examine micro- or nanocrystalline samples that resist single-crystal growth. Moving beyond isolated complexes, incorporating these metal ion–DOTA motifs into transition-metal-crosslinked biopolymer matrices will test their relevance for biomaterial engineering while systematic studies on other biologically important divalent ions (*e.g.* Fe(II), Mn(II) and Cu(II)) and pendant-arm-modified DOTA analogues will further refine the structure–property relationships revealed here.

Experimental section

Chemicals and solvents were purchased from common vendors with analytical purity. DOTA was obtained from Chematech (France). Mass spectra were recorded using a Waters ACQUITY QDa MS detector (a part of the Waters Arc HPLC system) through a direct inlet. Samples were dissolved in water and inserted with 0.1% TFA in H_2O as a solvent and the MS data were processed using Empower 3 software. Elemental analyses were carried out at IOCB (Prague) by combustion analysis for C–H–N determination and by X-ray fluorescence for the other elements.

Diffraction data were collected at 120 K (Cryostream Cooler, Oxford Cryosystem) using a Bruker D8 VENTURE Kappa Duo PHOTON100 diffractometer with an IμS micro-focus-sealed tube using Mo-Kα ($\lambda = 0.71073$ Å) or Cu-Kα ($\lambda = 1.54178$ Å) radiation. Data were analysed using the SAINT (Bruker AXS Inc.) software package and subsequently corrected for absorption effects using the numerical method (SADABS). The structures were solved using direct methods (SHELXT2018/2)[55] and refined with full-matrix least-squares techniques (SHELXL2019/2).[56] All non-hydrogen atoms were refined anisotropically. All hydrogen atoms were found in the difference density map. However, hydrogen atoms bound to carbon atoms were fixed in theoretical positions using $U_{eq}(H) = 1.2U_{eq}(C)$ to keep the number of parameters low, and only hydrogen atoms bound to oxygen atoms were tried for full refinement. However, some heteroatom-bound hydrogen atoms were fixed in the original positions, as the geometry during the refinement was unstable and heteroatom–hydrogen bond distances became unrealistically long or short. More details on refinements of the diffraction data for the particular phases are given in the SI.

Solution ^{1}H NMR and ^{13}C{^{1}H} NMR were performed using a Bruker Avance III HD 400, a Bruker Avance III Neo 400 (resonance frequencies 400/101 MHz for ^{1}H/^{13}C, respectively) or a Varian Unity Inova 400 (VT experiments). All NMR spectra were recorded at 25 °C unless stated otherwise. Spectra were referenced on the ^{1}H and ^{13}C NMR signals of *t*-BuOH (1.24/30.29 ppm). For temperature calibration, a standalone sealed NMR tube containing 80% ethylene glycol in DMSO-d_6 (for temperatures higher than 20 °C) or 99.8% CD_3OD (for temperatures below 20 °C) was used. For the VT experiments, the metal complexes in their diprotonated form (*ca.* 20 mg) were dissolved/suspended in D_2O (0.5 ml, containing 0.1% v/v *t*BuOH) and increasing the pH value to ~10 using saturated aq. $Ba(OH)_2$ led to clear solutions. For low temperature experiments, up to 40% v/v CD_3OD was added to prevent freezing of the solution. Prior to each acquisition, the sample was left to equilibrate at the appropriate temperature for at least 15 min. Then, the D_2O deuterium signal was locked, the spectrometer was shimmed and ^{13}C{^{1}H} NMR spectra were recorded. The ^{13}C{^{1}H} spectra were referenced so that the pendant CH_2 resonance stayed at a constant chemical shift throughout the temperature series. This ensured that the high-temperature shift of the macrocycle CH_2 groups fell halfway between the low-temperature peaks. The spectra were then phase- and baseline-corrected. For each peak, its position and width at half-maximum height were obtained by line-shape analysis in MestReNova. The ^{113}Cd NMR spectrum was measured using a Bruker Avance III 600 (resonance frequency 133.1 MHz). The ^{199}Hg NMR spectrum was recorded using a Bruker Avance III Neo 400 (resonance frequency 71.5 MHz). The ^{113}Cd and ^{199}Hg NMR spectra were referenced using a unified Ξ_i scale to avoid the use of toxic primary references.

Solid-state ^{13}C{^{1}H} CP-ss-NMR spectra were recorded using a Bruker Avance III HD 500 NMR spectrometer (^{13}C resonance frequency 126 MHz) equipped with a 3.2 mm broad-band probe at a MAS frequency of 11 kHz. The ^{13}C NMR scale was calibrated with glycine as an external standard (176.03 ppm for the low-field carbonyl signal). The ^{15}N CP-ss-NMR spectra were recorded using a Bruker Avance NEO 700 MHz spectrometer (^{15}N resonance frequency 71 MHz) equipped with a 3.2 mm broad-band probe at a MAS frequency of 10 kHz. The ^{15}N scale was calibrated with glycine as an external standard (34.35 ppm). Samples were packed into 3.2 mm zirconia rotors. All spectra were Fourier transformed, phase- and baseline-corrected using MestReNova software. To improve the resolution of the ^{13}C and ^{15}N CP-ss-NMR spectra, the FIDs were zero-filled to 16k points. Spectra were deconvoluted in MestreNova to obtain chemical shifts, line widths, and areas under the peaks using $L/G = 0.8$ as a default parameter for all peaks.

The unit cell parameters of Ba[Zn(dota)]·5.5H_2O were fixed and all internal coordinates were subject to optimization with respect to the crystal-lattice energy by the PW DFT (plane-waves density-functional theory) implemented in the CASTEP code.[57–59] In the calculations, the disordered water molecule with the major occupancy in the X-ray structure was con-

sidered. The PBE[60] functional was applied together with the ZORA (the scalar-relativistic zeroth-order regular approximation) scheme[61] and with the "Fine" level of settings of the CASTEP version 16.1. In particular, the PW cut-off value was 571 eV and the Monkhorst–Pack grids[62] to sample the Brillouin zone were: $3 \times 1 \times 2$, no offset, 3 k-points. The optimized structures were then used to predict the NMR chemical shielding of ^{13}C nuclei. The same PBE–ZORA approach as employed in geometry optimizations was combined with the gauge-including projector augmented wave (GIPAW) method.[63,64] The CASTEP-NMR module was used.[56]

Synthesis of [M(H$_2$dota)] (M = Zn and Cd) complexes

H$_4$dota·2H$_2$O (0.50 g, 1.14 mmol) was weighed into a round-bottom flask (50 ml) and dissolved in water (25 ml). Then, the appropriate metal oxide (1 equiv.) was added, and the solution was stirred at 60 °C overnight. Gradual dissolution of the metal oxide was observed. Afterwards the suspension was filtered through a 0.22 μm PVDF microfilter and the volatiles were removed *in vacuo*. The residue was dissolved in water (10 ml), the solution was overlayered with acetone and the mixture was left to crystallize in a refrigerator. After several days, a colourless microcrystalline product was collected by filtration, washed with acetone and dried in air yielding [Zn(H$_2$dota)]·6H$_2$O (0.44 g, 83%) or [Cd(H$_2$dota)]·H$_2$O (0.57 g, 94%).

[Zn(H$_2$dota)]. ^{1}H NMR (D$_2$O, pH 9 (aq. NH$_3$), 400 MHz): 3.30 (s, 8H, NCH_2CO$_2$H), 3.17–3.03 (m, 8H, ring CH_2), 2.91–2.78 (m, 8H, ring CH_2). ^{13}C{^{1}H} NMR (D$_2$O, pH 9 (aq. NH$_3$), 101 MHz): 177.74 (CO), 59.25 (NCH$_2$CO$_2$H), 53.16 (ring CH$_2$). ESI-MS: (+) 467.27 (467.11 for [Zn(H$_3$dota)]$^+$); (−) 465.07 (465.10 for [Zn(Hdota)]$^-$). Elemental analysis, found (calcd for [Zn(H$_2$dota)]·6H$_2$O): C 33.8 (33.4), H 5.4 (6.7), N 9.7 (9.7).

[Cd(H$_2$dota)]. ^{1}H NMR (D$_2$O, pH 5.0, 400 MHz): 3.13 (8H, s, NCH_2CONH$_2$), 2.83 (8H, s, ring CH_2), 2.57 (8H, s, ring CH_2). ^{13}C{^{1}H} NMR (D$_2$O, pH 5.0, 101 MHz): 178.7 (CO, ^2J($^{113/111}$Cd–C) 8.7 Hz), 57.5 (CH$_2$CONH$_2$), 49.9 (ring CH$_2$). ^{113}Cd NMR (D$_2$O, pH ~12, LiOD): −562 ppm. ESI-MS: (+) 517.09 (517.09 for [Cd(H$_3$dota)]$^+$); (−) 514.68 (515.07 for [Cd(Hdota)]$^-$).

Synthesis of [Hg(H$_2$dota)]

Solid HgCl$_2$ (0.31 g, 1 equiv.) was dissolved in water (6 ml) and 1 M aq. LiOH (2 ml) was added resulting in the formation of a HgO precipitate. This suspension was centrifuged at 6000 rpm for 5 min and the clear supernatant was decanted off. The precipitated HgO was then washed with water (3 × 8 ml) by centrifugation. The freshly prepared HgO was re-suspended in water (5 ml) and the suspension was added into a hot (60 °C) solution of H$_4$dota·2H$_2$O (0.50 g, 1.14 mmol) in water (20 ml). The reaction mixture was stirred at 60 °C overnight to achieve a full complex formation. Afterwards, the suspension was diluted with water (~200 ml) and heated up to 95 °C for a short time. Then, the hot suspension was filtered through a fine frit and the filtrate was left to cool down. It was overlayered with acetone (50 ml) and the sample was stored in a fridge. Over a week, the formation of tiny colourless crystals

was observed. The crystals of [Hg(H$_2$dota)]·4H$_2$O were filtered off, washed with acetone and dried in air (0.50 g, 67%). ^{1}H NMR (D$_2$O, pH 5.0, 400 MHz): 3.34 (8H, s, NCH_2CO$_2$H), 2.86 (16H, s, ring CH_2). ^{13}C{^{1}H} NMR (D$_2$O, pH 5.0, 101 MHz): 176.9 (CO, ^2J(Hg–C) 18.4 Hz), 57.4 (CH$_2$CO$_2$H), 49.5 (ring CH$_2$). ^{199}Hg NMR (D$_2$O, pH ~12, LiOD): −1820 ppm. ESI-MS: (+) 605.36 (605.15 for [Hg(H$_3$dota)]$^+$); (−) 603.21 (603.14 for [Hg(Hdota)]$^-$). Elemental analysis, found (calcd for [Hg(H$_2$dota)]·4H$_2$O): C 28.7 (28.5), H 3.8 (5.1), N 8.2 (8.3), Hg 28.9 (29.7).

Synthesis of Ca[Hg(dota)]·9.5H$_2$O

[Hg(H$_2$dota)]·4H$_2$O (0.0200 g, 0.039 mmol) was suspended in water (0.5 ml) and solid Ca(OH)$_2$ (0.0025 g, 1 equiv.) was added. Upon addition of the hydroxide, the solution/suspension cleared up. The resulting light suspension was filtered through a 0.2 μm PVDF microfilter and the filtrate was collected into a vial which was placed in a closed vessel with acetone. Over several days, the Ca(II) salt crystallized (0.0317 g, 100%). The single crystals were chosen from the bulk material.

Synthesis of Ba[M(dota)]·nH$_2$O

The [M(H$_2$dota)]·nH$_2$O phase was suspended in water (5 ml) and saturated aq. Ba(OH)$_2$ (~1.1 equiv.) was added just to dissolve the complex. The light suspension was filtered through a 0.2 μm PVDF microfilter and the filtrate was collected into a vial which was placed in a closed vessel with acetone. Over several days (for the Cd(II)/Hg(II) complexes) or several weeks (for the Zn(II) complex), a solid crystalline material was formed. The crystals were filtered off, washed with acetone and dried in air. The single crystals were taken from the bulk, and this material was also used for ss-NMR measurements as soon as possible after the isolation. The Ba(II) salts slowly loose water from crystallization during storing.

Ba[Hg(dota)]·8.5H$_2$O. From [Hg(H$_2$dota)]·4H$_2$O (0.075 g, 0.11 mmol) and aq. Ba(OH)$_2$ (0.60 ml); yield 0.065 g (66%).

Ba[Cd(dota)]·12H$_2$O. From [Cd(H$_2$dota)]·H$_2$O (0.22 g, 0.41 mmol) and aq. Ba(OH)$_2$ (2.00 ml); yield 0.210 g (59%).

Ba[Zn(dota)]·5.5H$_2$O. From [Zn(H$_2$dota)]·6H$_2$O (0.25 g, 0.43 mmol) and aq. Ba(OH)$_2$ (2.88 ml); yield 0.144 g (47%).

Author contributions

J. O.: synthesis and characterization of all complexes; I. C.: X-ray diffraction data acquisition; J. O. and I. C.: fitting the X-ray data; J. O. and J. B.: ss-NMR spectral measurements and interpretation; J. B.: theoretical calculations; and P. H.: the study concept and interpretation of solution NMR data. All authors participated in the manuscript writing.

Conflicts of interest

There are no conflicts to declare.

Data availability

The data supporting this article have been included as part of the supplementary information (SI). Supplementary information: extended discussion of solid-state structures determined by X-ray diffraction, tables with structural parameters and experimental details of X-ray diffraction studies; figures of ^{13}C and ^{15}N ss-NMR spectra, tables with results of deconvolution of these ss-NMR spectra and assignment of the ^{13}C ss-NMR spectra; figures of solution NMR spectra at various temperatures and tables with results of fitting of variable-temperature solution NMR data; ^{113}Cd and ^{199}Hg solution NMR spectra. See DOI: https://doi.org/10.1039/d5dt01880c.

CCDC 2477250–2477254 contain the supplementary crystallographic data for this paper.[65a–e]

References

1 P. Hermann, J. Kotek, V. Kubíček and I. Lukeš, *Dalton Trans.*, 2008, 3027–3047.
2 J. Wahsner, E. M. Gale, A. Rodríguez-Rodríguez and P. Caravan, *Chem. Rev.*, 2019, **119**, 957–1057.
3 A. Boros and A. B. Packard, *Chem. Rev.*, 2019, **119**, 870–901.
4 T. I. Kostelnik and C. Orvig, *Chem. Rev.*, 2019, **119**, 902–956.
5 L. Bodei, K. Herrmann, H. Schöder, A. M. Scott and J. S. Lewis, *Nat. Rev. Clin. Oncol.*, 2022, **19**, 534–550.
6 E. Mathieu, A. Sipos, E. Demeyere, D. Phipps, D. Sakaveli and K. E. Borbas, *Chem. Commun.*, 2018, **54**, 10021–10035.
7 D. Parker, J. D. Fradgley and K. L. Wong, *Chem. Soc. Rev.*, 2021, **50**, 8193–8213.
8 E. de Kerviler, K. Maravilla, J.-F. Meder, O. Naggara, C. Dubourdieu, V. Jullien and P. Desché, *Invest. Radiol.*, 2016, **51**, 544–551.
9 U. Hennrich and M. Benešová, *Pharmaceuticals*, 2020, **13**, 38.
10 L. Urso, A. Nieri, L. Uccelli, A. Castello, P. Artioli, C. Cittanti, M. C. Marzola, L. Florimonte, M. Castellani, S. Bissoli, F. Porto, A. Boschi, L. Evangelista and M. Bartolomei, *Pharmaceutics*, 2023, **15**, 1110.
11 O. Sartor, J. de Bono, K. N. Chi, K. Fizazi, K. Herrmann, K. Rahbar, S. T. Tagawa, L. T. Nordquist, N. Vaishampayan, G. El-Haddad, C. H. Park, T. M. Beer, A. Armour, W. J. Perez-Contreras, M. DeSilvio, E. Kpamegan, G. Gericke, R. A. Messmann, M. J. Morris and B. J. Krause, *N. Engl. J. Med.*, 2021, **385**, 1091–1103.
12 N. Viola-Villegas and R. P. Doyle, *Coord. Chem. Rev.*, 2009, **253**, 1906–1925.
13 J. Martinelli, B. Balali-Mood, R. Panizzo, M. F. Lythgoe, A. J. P. White, P. Ferretti, J. H. G. Steinke and R. Vilar, *Dalton Trans.*, 2010, **39**, 10056–10067.
14 N. Bernier, J. Costa, R. Delgado, V. Félix, G. Royal and R. Tripier, *Dalton Trans.*, 2011, 4514–4526.
15 T. S. Robinson, O. Wyness, S. F. Lincoln, M. R. Taylor, E. R. T. Tiekink and K. P. Wainwright, *Inorg. Chim. Acta*, 2006, **359**, 1413–1420.
16 H. Maumela, R. D. Hancock, L. Carlton, J. H. Reibenspies and K. P. Wainwright, *J. Am. Chem. Soc.*, 1995, **117**, 6698–6707.
17 G. de Martino Norante, M. Di Vaira, F. Mani, S. Mazzi and P. A. Stoppioni, *Inorg. Chem.*, 1990, **29**, 2822–2829.
18 S. Aoki, H. Kawatani, T. Goto, E. Kimura and M. Shiro, *J. Am. Chem. Soc.*, 2001, **123**, 1123–1132.
19 G. S. Tsebrikova, I. N. Polyakova, V. P. Solovev, I. S. Ivanova, I. P. Kalashnikova, G. E. Kodina, V. E. Baulin and A. Yu. Tsivadze, *Inorg. Chim. Acta*, 2018, **478**, 250–259.
20 A. Riesen, M. Zehnder and T. A. Kaden, *Acta Crystallogr., Sect. C: Cryst. Struct. Commun.*, 1991, **47**, 531–533.
21 B. B. Correia, T. R. Brown, J. H. Reibenspies, H. Lee and R. D. Hancock, *Inorg. Chim. Acta*, 2020, **506**, 119544.
22 S. Amatori, G. Ambrosi, E. Borgogelli, M. Fanelli, M. Formica, V. Fusi, L. Giorgi, E. Macedi, M. Micheloni, P. Paoli, P. Rossi and A. Tassoni, *Inorg. Chem.*, 2014, **53**, 4560–4569.
23 J. Barreto, T. Joshi, T. K. Venkatachalam, D. C. Reutens, B. Graham and L. Spiccia, *J. Coord. Chem.*, 2015, **68**, 335–349.
24 C. B. Smith, S. F. Lincoln, M. R. Taylor and K. P. Wainwright, *Acta Crystallogr., Sect. C: Cryst. Struct. Commun.*, 2003, **59**, m358–m360.
25 P. J. Davies, S. F. Lincoln, C. B. Smith, M. R. Taylor, K. P. Wainwright and K. S. Wallwork, *Acta Crystallogr., Sect. C: Cryst. Struct. Commun.*, 2000, **56**, 28–30.
26 C. B. Smith, A. K. W. Stephens, K. S. Wallwork, S. F. Lincoln, M. R. Taylor and K. P. Wainwright, *Inorg. Chem.*, 2002, **41**, 1093–1100.
27 M. Di Vaira, F. Mani, M. Menicatti, R. Morassi and P. Stoppioni, *Polyhedron*, 1997, **16**, 3585–3591.
28 R. D. Hancock, J. H. Reibenspies and H. Maumela, *Inorg. Chem.*, 2004, **43**, 2981–2987.
29 M. Tosato, P. Randhawa, M. Asti, L. B. S. Hemmingsen, C. A. O'Shea, P. Thaveenrasingam, S. P. A. Sauer, S. Chen, C. Graiff, I. Menegazzo, M. Baron, V. Radchenko, C. F. Ramogida and V. Di Marco, *Inorg. Chem.*, 2024, **63**, 14241–14255.
30 A. K. W. Stephens, R. Dhillon, S. F. Lincoln and K. P. Wainwright, *Inorg. Chim. Acta*, 1995, **236**, 185–188.
31 M. Di Vaira, F. Mani, S. S. Costantini, P. Stoppioni and A. Vacca, *Eur. J. Inorg. Chem.*, 2003, 3185–3192.

32 A. Riesen, M. Zehnder and T. A. Kaden, *J. Chem. Soc., Chem. Commun.*, 1985, 1336–1338.

33 A. Riesen, M. Zehnder and T. A. Kaden, *Helv. Chim. Acta*, 1986, **69**, 2067–2073.

34 A. Riesen, M. Zehnder and T. A. Kaden, *Helv. Chim. Acta*, 1986, **69**, 2074–2080.

35 S. Wang and T. D. Westmoreland, *Inorg. Chem.*, 2009, **48**, 719–727.

36 R. Uzal-Varela, F. Perez-Fernandez, L. Valencia, A. Rodriguez-Rodriguez, C. Platas-Iglesias, P. Caravan and D. Esteban-Gomez, *Inorg. Chem.*, 2022, **61**, 14173–14186.

37 A. Heppeler, J. P. André, I. Buschmann, X. Wang, J.-C. Reubi, M. Hennig, T. A. Kaden and H. R. Maecke, *Chem. – Eur. J.*, 2008, **14**, 3026–3034.

38 L. Burai, E. Tóth, G. Moreau, A. Sour, R. Scopelliti and A. E. Merbach, *Chem. – Eur. J.*, 2003, **9**, 1394–1404.

39 J. Brus, M. Urbanová, J. Czernek, M. Pavelková, K. Kubova, J. Vysloužil, S. Abbrent, R. Konefal, J. Horský, D. Vetchý, J. Vysloužil and P. Kulich, *Biomacromolecules*, 2017, **18**, 2478–2488.

40 M. Urbanová, J. Macků, K. Kubová, J. Vysloužil, J. Muselík, M. Šlouf, I. Sedenková, O. Kocková, L. Janisová, J. Mašek, E. Mašková, A. Novobilský, M. Parenicová, R. Konefal, I. Czernek, D. Vetchý, M. Pavelková and J. Brus, *Food Hydrocolloids*, 2024, **150**, 109693.

41 J. Vícha, J. Novotný, S. Komorovský, M. Straka, M. Kaupp and R. Marek, *Chem. Rev.*, 2020, **120**, 7065–7103.

42 B. Zhang, Y. Zhou, H.-Y. Huang, X.-L. Zhang, Y. Xiang, Y. Shi, C. Zhang, A. Yuan, X. Cai, L. Chen, Y.-Q. Zhang and Z.-B. Hu, *Inorg. Chem. Front.*, 2024, **11**, 2648–2660.

43 C. B. Smith, K. S. Wallwork, J. M. Weeks, M. A. Buntine, S. F. Lincoln, M. R. Taylor and K. P. Wainwright, *Inorg. Chem.*, 1999, **38**, 4986–4992.

44 C. B. Smith, S. F. Lincoln, M. R. Taylor and K. P. Wainwrigh, *Acta Crystallogr., Sect. E: Struct. Rep. Online*, 2002, **58**, m33–m35.

45 P. Vojtíšek, P. Cígler, J. Kotek, J. Rudovský, P. Hermann and I. Lukeš, *Inorg. Chem.*, 2005, **44**, 5591–5599.

46 P. Urbanovský, J. Kotek, I. Císařová and P. Hermann, *Dalton Trans.*, 2020, **49**, 1555–1569.

47 M. Tosato, L. Lazzari and V. Di Marco, *ACS Omega*, 2022, **7**, 15596–15602.

48 E. Csajbók, Z. Baranyai, I. Bányai, E. Brücher, R. Király, A. Müller-Fahrnow, J. Platzek, B. Radüchel and M. Schaffer, *Inorg. Chem.*, 2003, **42**, 2342–2349.

49 T. Fodor, I. Bányai, A. Bényei, C. Platas-Iglesias, M. Purgel, G. L. Horváth, L. Zékány, G. Tircsó and I. Tóth, *Inorg. Chem.*, 2015, **54**, 5426–5437.

50 E. N. Zapolotsky, Y. Qu and S. P. Babailov, *J. Inclusion Phenom. Macrocyclic Chem.*, 2022, **102**, 1–33.

51 K. D. M. Harris, *Crystals*, 2022, **12**, 1277.

52 S. Sneddon, J. Kahr, A. F. Orsi, D. J. Price, D. M. Dawson, P. A. Wright and S. E. Ashbrook, *Solid State Nucl. Magn. Reson.*, 2017, **87**, 54–64.

53 N. Asakawa, S. Kuroki, H. Kurosu, I. Ando, A. Shoji and T. Ozaki, *J. Am. Chem. Soc.*, 1992, **114**, 3261–3265.

54 A. Kondoh and T. Oi, *Z. Naturforsch.*, 1998, **53**, 77–91.

55 G. M. Sheldrick, *Acta Crystallogr., Sect. A: Found. Adv.*, 2015, **71**, 3–8.

56 J. Lübben, C. M. Wandtke, C. B. Hübschle, M. Ruf, G. M. Sheldrick and B. Dittrich, *Acta Crystallogr., Sect. A: Found. Adv.*, 2019, **75**, 50–62.

57 G. Kresse and D. Joubert, *Phys. Rev. B*, 1991, **59**, 1758–1775.

58 M. D. Segall, P. J. D. Lindan, M. J. Probert, C. J. Pickard, P. J. Hasnip, S. J. Clark and M. C. Payne, *J. Phys.: Condens. Matter*, 2002, **14**, 2717–2744.

59 S. J. Clark, M. D. Segall, C. J. Pickard, P. J. Hasnip, M. I. J. Probert, K. Refson and M. C. Payne, *Z. Kristallogr.*, 2005, **220**, 567–570.

60 J. P. Perdew, K. Burke and M. Ernzerhof, *Phys. Rev. Lett.*, 1996, **77**, 3865–3868.

61 J. R. Yates, C. J. Pickard, M. C. Payne and F. Mauri, *J. Chem. Phys.*, 2003, **118**, 5746–5753.

62 H. J. Monkhorst and J. D. Pack, *Phys. Rev. B*, 1976, **13**, 5188–5192.

63 J. R. Yates, C. J. Pickard and F. Mauri, *Phys. Rev. B*, 2007, **76**, 024401.

64 C. J. Pickard and F. Mauri, *Phys. Rev. B*, 2001, **63**, 245101.

65 (*a*) CCDC 2477250: Experimental Crystal Structure Determination, 2025, DOI: 10.5517/ccdc.csd.cc2p4s9y; (*b*) CCDC 2477251: Experimental Crystal Structure Determination, 2025, DOI: 10.5517/ccdc.csd.cc2p4sbz; (*c*) CCDC 2477252: Experimental Crystal Structure Determination, 2025, DOI: 10.5517/ccdc.csd.cc2p4sc0; (*d*) CCDC 2477253: Experimental Crystal Structure Determination, 2025, DOI: 10.5517/ccdc.csd.cc2p4sd1; (*e*) CCDC 2477254: Experimental Crystal Structure Determination, 2025, DOI: 10.5517/ccdc.csd.cc2p4sf2.